Int. J. Heat Mass Transfer. Vol. 29, No. 6, pp. 841–853, 1986
Printed in Great Britain

0017–9310/86 $3.00 + 0.00
Pergamon Journals Ltd.

Numerical study of natural convection in a vertical, porous annulus with constant heat flux on the inner wall

V. PRASAD
Department of Mechanical Engineering, Columbia University, New York, NY 10027, U.S.A.

(*Received* 12 *August* 1985 *and in final form* 5 *December* 1985)

Abstract—Numerical solutions for natural convection in a vertical, porous annulus are reported for the case when the inner wall is heated by applying a constant heat flux. This results in a higher rate of heat transfer compared to the isothermal heating. The higher the aspect ratio, the larger is this difference whereas the effect of radius ratio is just the reverse. Though the heat transfer rate increases with the curvature, the exponent p in $Nu = C\,\overline{Ra}^{*m} A^{-n} \kappa^{p}$, is a strong function of the radius ratio, κ. In the boundary-layer regime, p decreases logarithmically from a peak value at $\kappa = 1$. This brings the annulus results close to the cylinder solutions at large radius ratios. The peak temperature in the enclosure never exceeds twice the mean temperature.

1. INTRODUCTION

CONVECTIVE heat transfer in differentially heated, vertical, annular enclosures filled with saturated, porous media is a topic of many recent investigations owing to its importance in several geophysical and technological applications. Consequently, several analytical, numerical and experimental investigations have been reported for a vertical, concentric annulus whose inner wall is heated and whose outer wall is isothermally cooled, the top and bottom being insulated [1–9]. Though the experiments have been conducted for both the constant temperature [7, 8] and the constant heat flux [4, 9] boundary conditions, the theoretical studies are limited to only the isothermally heated inner wall [1–3, 5–7]. A detailed review of these works has recently been presented by Prasad *et al.* [9].

The purpose of the present work is to study numerically the natural convection in a vertical annulus filled with a saturated, porous medium when its inner wall is heated by applying a constant heat flux. To examine, the effects of the heated wall boundary condition on the temperature and flow fields, the local heat transfer rates and the overall Nusselt numbers, calculations have been made for wide range of governing parameters. The effects of these parameters on the peak temperature in the enclosure have also been studied in order to obtain an upper bound. Results have been further analyzed to characterize the situations when the heat transfer in an annulus is close to that for a vertical cylinder embedded in an infinite medium.

2. FORMULATION

Consider a fluid-saturated, porous layer enclosed by two concentric cylinders whose inner wall is heated by applying a constant heat flux and the outer wall is isothermally cooled, the top and bottom being insulated (Fig. 1). In the porous medium, Darcy's law is assumed to hold, the fluid is assumed to be a normal Boussinesq fluid, and the viscous drag and inertia terms in the equations of motion are neglected because their magnitudes are of small order compared to other terms for low Darcy numbers and low particle Reynolds numbers.

With the above assumptions, the conservation equations for mass, momentum and energy for steady, axi-symmetric flow in a homogeneous, isotropic, porous medium reduce to [6]

$$A^2 \frac{\partial}{\partial R}\left[\frac{1}{(\gamma R+1)}\frac{\partial \psi}{\partial R}\right] + \frac{\partial}{\partial Z}\left[\frac{1}{(\gamma R+1)}\frac{\partial \psi}{\partial Z}\right] = \overline{Ra}^{*} A \frac{\partial \theta}{\partial R} \quad (1)$$

$$\frac{\partial \psi}{\partial R}\frac{\partial \theta}{\partial Z} - \frac{\partial \psi}{\partial Z}\frac{\partial \theta}{\partial R} = \frac{\partial}{\partial R}\left[(\gamma R+1)\frac{\partial \theta}{\partial R}\right] + \frac{1}{A^2}\frac{\partial}{\partial Z}\left[(\gamma R+1)\frac{\partial \theta}{\partial Z}\right]. \quad (2)$$

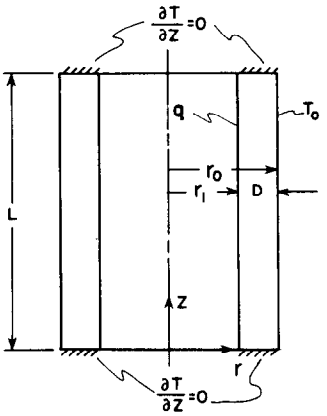

FIG. 1. Vertical annulus, coordinate system and thermal boundary conditions (q is uniform heat flux applied on the inner wall).

NOMENCLATURE

A aspect ratio, L/D
c specific heat of fluid at constant pressure [J kg^{-1} K^{-1}]
C constant for equation (7)
D gap width of porous annulus, $r_o - r_i$ [m]
g acceleration due to gravity [m s^{-2}]
h heat transfer coefficient on inner wall [W m^{-2} K^{-1}]
$\bar{h}$ average heat transfer coefficient on vertical wall [W m^{-2} K^{-1}]
K permeability of porous medium [m^2]
k effective thermal conductivity of the saturated porous medium [W m^{-1} K^{-1}]
L height of porous medium [m]
N number of iterations
Nu_z local Nusselt number on heated wall, hz/k
Nu average Nusselt number, $\bar{h}D/k$
P pressure [Pa]
Pr^* Prandtl number, ν/α
q constant heat flux applied on the inner wall [W m^{-2}]
Q heat transfer rate [W]
r radial coordinate [m]
R dimensionless radial distance, $(r - r_i)/D$
Ra^* Rayleigh number, $(g\beta K D\Delta T)/(\nu\alpha)$
$\overline{Ra}^*$ Rayleigh number based on heat flux, $(g\beta K D^2 q)/(\nu\alpha k)$
T temperature [K]
ΔT temperature difference across annulus [K]; $(T_i - T_o)$, for constant temperature, and $(T_{m,i} - T_o)$, for constant flux heating
u fluid velocity in r-direction, $-[\alpha/D(\gamma R+1)](\partial\psi/\partial Z)$[m s^{-1}]
v fluid velocity in z-direction, $[\alpha L/D^2(\gamma R+1)](\partial\psi/\partial R)$[m s^{-1}]
z axial coordinate [m]
Z dimensionless axial distance, z/L.

Greek symbols
α thermal diffusivity of porous medium $k/\rho c$, [m^2 s^{-1}]
β isobaric coefficient of thermal expansion of fluid [K^{-1}]
γ radius ratio parameter, $D/r_i = \kappa - 1$
θ dimensionless temperature $(T - T_o)/(qD/k)$
ν kinematic viscosity of fluid [m^2 s^{-1}]
κ radius ratio, r_o/r_i
ρ density of fluid [kg m^{-3}]
ψ' streamfunction
ψ dimensionless streamfunction, $(D/\alpha r_i L)\psi'$.

Subscripts
cond conduction
cyl cylinder embedded in an infinite porous medium
i inner wall (heated)
iso isothermally heated annulus
l local value
L based upon annulus height, L
m mean on the inner wall
max maximum
o outer wall (cold)
r_o based on outer radius, r_o
w wall.

The relevant hydrodynamic and thermal boundary conditions are:

$$\psi = 0, \quad \partial\theta/\partial R = -1 \quad \text{at} \quad R = 0 \tag{3a}$$

$$\psi = 0, \quad \theta = 0 \quad \text{at} \quad R = 1 \tag{3b}$$

$$\psi = 0, \quad \partial\theta/\partial Z = 0 \quad \text{at} \quad Z = 0 \text{ and } Z = 1. \tag{3c}$$

It may be noted that the above approach of formulating the vertical annulus problem and introducing the dimensionless parameters reduces the present problem to a vertical cavity just by substituting $\gamma = 0$ or $\kappa = 1$. The advantage of the present formulation is that the vertical annulus can simply be treated as an extension of the rectangular cavity where an additional geometric parameter, the radius ratio needs to be considered.

3. NUMERICAL METHOD

Finite-difference equations are derived from equations (1) and (2) by integration over finite area elements, following a procedure outlined by Gosman *et al.* for axi-symmetric flows [11]. This introduces upwind differences for the convective terms in the energy equation. The successive substitution formulae derived in this way satisfy the convergence criteria and are quite stable for many circumstances [11, 12]. For solving the system of algebraic equations thus obtained, a point iterative method is used. The solution technique is well described in the literature and has been widely used for recirculating flows. The applicability of the method and its accuracy for the convective heat transfer in annular and rectangular enclosures has already been discussed elsewhere [6, 10].

For the present work, uniform mesh sizes have been used for both x- and y-directions provided the Rayleigh number is small, usually less than 200. For moderately high and high Rayleigh numbers ($\overline{Ra}^* > 200$), non-uniform grids with fine mesh near the walls, are used. For the trial cases, the selected mesh sizes gave the average Nusselt numbers within 2% of the asymptotic values predicted by the calculations with much finer

grids when $\overline{Ra}^*$ and κ are not very large. For high Rayleigh numbers, $\overline{Ra}^* > 2000$ and large radius ratios, $\kappa \geqslant 10$, a variation of 3% has been accepted to keep the computational costs low. The following are the grid fields used for the present calculations:

A	1,2	5	10	20
Grid field	31×31	31×41	27×41	21×41 or 27×41.

In general, the over-relaxation of temperature helps in obtaining faster convergence. The over-relaxation parameter varies from 1.95 to 1 when $\overline{Ra}^*$ is increased from a very low to high values. At high Rayleigh numbers, $\overline{Ra}^* \geqslant 2000$, the under-relaxation of the streamfunction is more helpful. Based on the trial results for various combinations of $\overline{Ra}^*$, A and κ, a convergence criterion of 0.05% or lesser change in both θ and ψ at all nodes in the domain has been selected to test the convergence of the iterative scheme.

To further check the accuracy of the numerical results, an overall energy balance has been used for the system which compares the heat rejected at $r = r_o$ to the energy input at $r = r_i$. Generally, the energy balance is achieved within 2%. However, for large values of $\overline{Ra}^*$ and κ, the results have been accepted if the energy balance is satisfied within 4%.

To select a suitable representation for the constant flux boundary condition on the heated wall, the computations were done with two-, three-, four- and five-point derivatives for various combinations of $\overline{Ra}^*$, A and κ (Table 1). It was observed that a four-point derivative produces better energy balance across the enclosure, compared to two- and three-point derivatives without any appreciable impact on the convergence rate. A five-point derivative resulted in a marginal improvement over the four-point derivative. Hence, for the present computations, the four-point derivative (3rd-order accurate) has been used for the zero and constant heat flux boundary conditions.

Another important aspect of the present computational scheme is that 2–3 times more CPU time is required for the constant heat flux boundary condition compared to that for the constant temperature case. A detailed discussion on the other aspects of the present computational technique are presented in refs. [6, 10].

Table 1. Effects of two-, three-, four-, and five-point derivatives on the computational results

	$\overline{Ra}^*$	10^2	2×10^3	2×10^3	10^4
	A	1	1	10	5
	κ	2	10	20	2
Two points	N†	283	324	131	307
	%E†	10.24	12.29	12.54	12.11
	Nu	2.524	11.108	8.556	10.510
Three points	N	296	328	152	310
	%E	1.35	3.08	2.32	3.69
	Nu	2.655	11.739	9.227	11.054
Four points	N	300	331	157	313
	%E	0.33	2.00	0.59	2.85
	Nu	2.670	11.814	9.356	11.103
Five points	N	304	335		
	%E	0.14	1.85		
	Nu	2.672	11.820		

† N: number of iterations, E: energy balance.

4. RESULTS AND DISCUSSION

Numerical results for a vertical annulus with constant heat flux on the inner wall, have been obtained for wide range of Rayleigh number, aspect ratio and radius ratio. To examine the effects of the heated wall boundary conditions, these results have been compared with the heat transfer data for the isothermal heating, either obtained from ref. [6] or recalculated to match the corresponding values of Ra^*, A and κ. Since the present results for $A = 14.4, \kappa = 3.5$ and $A = 11.08$, $\kappa = 14$ have already been compared with the experimental data elsewhere [9], no attempt has been made here to compare the two results. The primary objectives of the present study are to characterize the effects of the curvature and the heated wall boundary condition.

4.1. *Temperature and flow fields*

It is now well-established that the introduction of curvature effects disturbs the centro-symmetric property of the temperature and flow fields observed in the case of an isothermally heated, vertical cavity ($\kappa = 1$) [1, 2, 5–7]. For fixed values of Ra^* and A, an increase in radius ratio produces a large temperature gradient near the hot wall, and a strongly stratified medium in the upper region of the annulas [6, 7]. The larger the radius ratio, the stronger is the convective flow near the top edge of the cooled wall, which results in a shift of the so-called core from the central region to the right top corner [6].

In the case of a vertical cavity ($\kappa = 1$), the change in the boundary condition from the constant temperature to a uniform heat flux produces very similar effects on the temperature and velocity fields [10]. It is thus reasonable to expect that the curvature effects combined with the constant heat flux boundary condition will produce much stronger asymmetric behavior, and will result in a larger temperature drop across the inner boundary layer and higher velocities in the top right corner.

In order to facilitate a direct comparison between the temperature and flow fields for the isothermal and uniform flux heating, the isotherms and streamlines for $Ra^* \simeq 10^3$ ($\overline{Ra}^* = 2.8 \times 10^4$), $A = 1$ and $\kappa = 6$ are presented in Fig. 2. These values of Ra^*, A and are the same as those for ref. [6, Fig. 2c]. It is observed that a change in the boundary condition from the constant temperature to a constant heat flux has resulted in a much thinner thermal boundary layer on the inner wall. This produces a thicker cold layer in the bottom region and a stronger stratification in the upper layers. The effective sink temperature for this boundary layer has thus decreased which results in a higher rate of heat

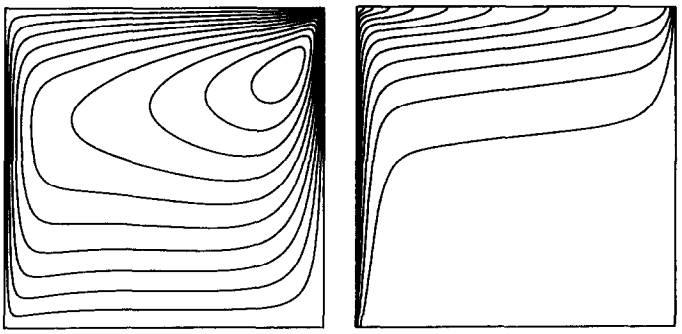

FIG. 2. Streamlines and isotherms for $\overline{Ra}^* = 2.8 \times 10^4$ ($Ra^* \simeq 10^3$), $A = 1$ and $\kappa = 6$ ($\Delta\theta = 0.005$, $\Delta\psi = 5$); Compare with Fig. 2c in ref. [6].

transfer for the constant flux heating; 8% increase over the isothermal heating for the present values of Ra^*, A and κ (Fig. 2). An average temperature outside the boundary layer may be considered as the effective sink temperature for the present discussion.

This sharp drop in temperature across the inner boundary layer may also be observed in Fig. 3, where the dimensionless temperature, θ, is plotted against R for $\overline{Ra}^* = 10^3$ and 10^4, and $\kappa = 2$, 5 and 20. The temperature at mid-height drops to less than 25% of its wall value, θ_w, within 20% of the cavity width when $\overline{Ra}^* = 10^4$ and $\kappa = 2$. If κ is increased to 20, the drop in temperature may be as large as 82% within the same distance from the inner wall. When both the Rayleigh number and the radius ratio are large, the stratification in the upper layers is so strong that θ/θ_w drops to a very small value in a large portion of the annulus, for example, $\theta/\theta_w < 0.25$ for $R > 0.2$ and $Z < 0.85$ when $\overline{Ra}^* = 10^4$ and $\kappa = 20$ (Fig. 3).

Any increase in Rayleigh number further strengthens the stratification in the upper region and results in a larger temperature gradient on the hot wall (Fig. 3). Qualitatively, the effects of $\overline{Ra}^*$ and A are very similar to what have already been reported for the isothermally heated annulus [1, 2, 5–7].

The above asymmetric behavior of the temperature field results in a flow field where the velocities are quite large near the top edge of the cold wall, and are very small in the lower region (Fig. 2). The center of the core (a point of zero velocity) has moved toward the right top corner producing a strong velocity boundary layer on the cold wall. This behavior is further strengthened by an increase in $\overline{Ra}^*$ and/or κ [6, 7].

4.2. *Heated wall temperature*

Since the temperature distribution on the heated wall and the peak temperature, θ_w at $R = 0$, $Z = 1$, are of considerable importance in the case of constant flux heating, the dimensionless wall temperature, θ_w, is plotted against Z in Fig. 4. An increase in Rayleigh number beyond zero (conduction) distorts the horizontal temperature profile (Fig. 4a) in such a way that θ_w decreases in the lower portion of the heated wall, and increases in the upper region. In general, θ_w at any location is observed to decrease with an increase in $\overline{Ra}^*$ (Fig. 4). This does not mean that the actual temperature,

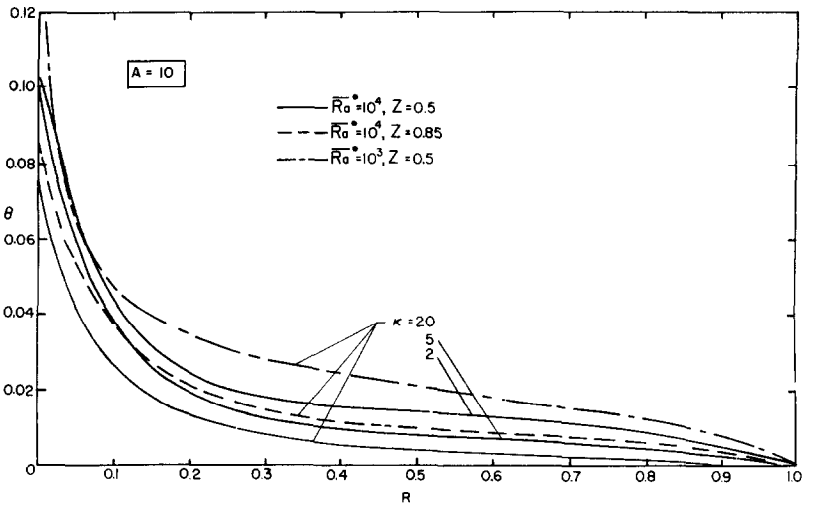

FIG. 3. Effects of Rayleigh number and radius ratio on temperature distributions at $Z = 0.5$ and 0.85.

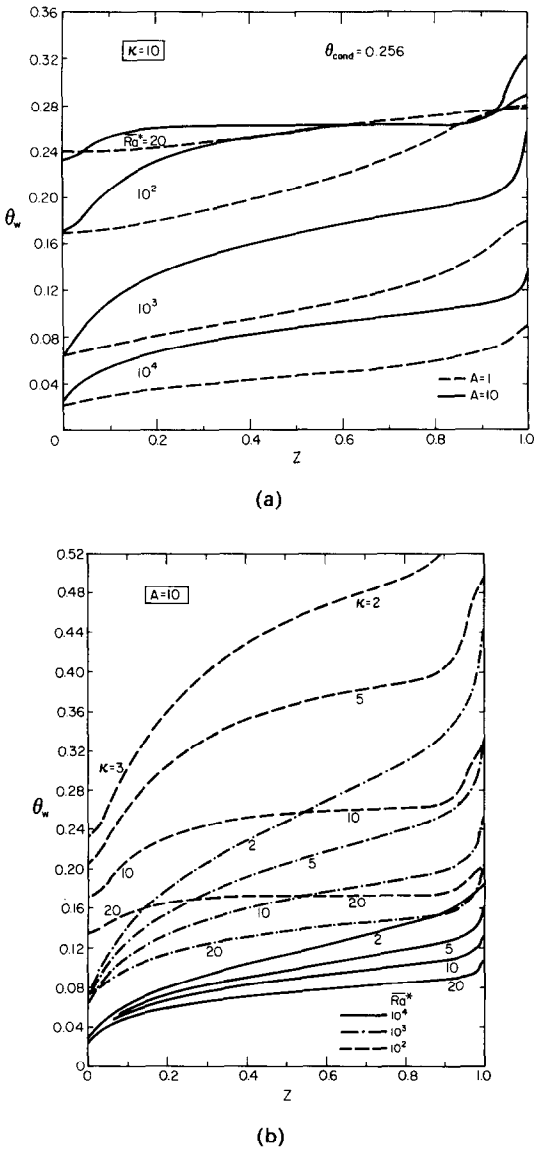

FIG. 4. Variation in heated wall temperature for various Rayleigh numbers, for (a) $\kappa = 10$ and (b) $A = 10$.

T_w, continually decreases when $\overline{Ra}^*$ is increased. It is interesting to find out the effects of power input, q, cavity width, D, permeability, K, and the thermophysical properties, ν, ρ_f, β, c and k on the wall temperature, T_w. From the definition of $\overline{Ra}^*$ it is clear that if the Rayleigh number is increased by changing the thermophysical properties, ν, ρ_f, β, c, and the permeability, K, the temperature, T_w at any given location will decrease. This is primarily due to the enhancement in heat carrying capacity of the fluid at high $\overline{Ra}^*$. On the other hand, if the Rayleigh number is enhanced by increasing q or D, or by decreasing k, the actual wall temperature will increase. The rate of change (increase or decrease) in the wall temperature, T_w, is a strong function of the Rayleigh number. The higher the Rayleigh number, the smaller is the rate of change in T_w (Fig. 4).

Generally, the temperature, θ_w, at any given location Z, increases with A (Fig. 4a), the change being minimal at $Z = 0$. Owing to the low velocities in the left top corner and the adiabatic boundary condition at the top wall, the temperature gradient, $\partial\theta_w/\partial Z$, near the top edge is much sharper for larger aspect ratios. Furthermore, for any fixed values of $\overline{Ra}^*$ and A, the dimensionless temperature, θ_w, decreases substantially with the increase in curvature (Fig. 4b) primarily because an increase in radius ratio for fixed D is always associated with an enhancement in the ratio of outer and inner surface areas. Another interesting effect of the radius ratio is the smoothening of temperature profile. The temperature gradient, $\partial\theta_w/\partial Z$, is observed to decrease with an increase in κ. For low $\overline{Ra}^*$, the temperature, θ_w, is almost constant for a large portion of the inner wall when the radius ratio is large (see the curve for $\overline{Ra}^* = 10^2$, $\kappa = 20$). Even at high Rayleigh numbers, such as $\overline{Ra}^* = 10^4$, the gradient $\partial\theta_w/\partial Z$ is very small when the curvature effects are strong. The sharp temperature gradients near the top and bottom edges are also modified by an increase in κ (Fig. 4b).

From the above discussion, it can be easily concluded that the peak temperature, θ_{max}, increases with the Rayleigh number and/or the aspect ratio, but continually decreases with an increase in radius ratio. Since the mean temperature on the heated wall, θ_m, is usually known (to be discussed later), an appropriate way to study the variation in θ_{max} may be to consider a normalized peak temperature θ_{max}/θ_m. The tabulated values of θ_{max}/θ_m (Table 2), indicate that the normalized peak temperature continually increases with $\overline{Ra}^*$, but decreases with an enhancement in the curvature. The effect of aspect ratio is not straight-forward. Depending on $\overline{Ra}^*$, there exists an aspect ratio for which the peak temperature is the largest. The higher the Rayleigh number, the smaller is the aspect ratio for $(\theta_{max}/\theta_m)_{max}$ (Table 2). For the present range of parameters the

Table 2. Variation in the normalized peak temperature, θ_{max}/θ_m

		$\overline{Ra}^*$						$\overline{Ra}^*$			
A	κ	20	10^2	10^3	10^4	κ	A	20	10^2	10^3	10^4
	2	1.330	1.548	1.804	1.805		1	1.125	1.387	1.734	1.930
	3	1.269	1.489	1.743	1.743		2	1.221	1.511	1.811	1.879
10	5	1.192	1.413	1.665	1.665	5	5	1.231	1.532	1.762	1.768
	10	1.107	1.303	1.565	1.574		10	1.192	1.413	1.665	1.665
	20	1.055	1.203	1.389	1.502		20	1.145	1.291	1.479	1.594

normalized peak temperature is maximum when $\overline{Ra}^* = 10^4$ and $\kappa = 1$. The upper bound for this temperature ratio is, thus, 1.932 which exists at $A = 1$ [10]. In general, the peak temperature, θ_{max}, will never exceed $2\theta_m$ as long as $\overline{Ra}^* \leqslant 10^4$ and $A \geqslant 1$.

4.3. *Local heat transfer rate*

A quantity of practical interest is the local heat flux on the cold wall,

$$q_l/q = -\partial\theta/\partial R \quad \text{at} \quad R = 1. \tag{4}$$

This normalized local heat flux is presented in Fig. 5 for $A = 1$ and 10. It is observed that a large percentage of heat is rejected within a small distance from the top edge when the radius ratio is small. An increase in radius ratio results in lower heat flux near the top edge whereas an increase in aspect ratio has the reverse effect. The taller the cavity, the larger is the fraction of heat rejected near the top edge (Fig. 5). The local heat flux in the top region further increases with the Rayleigh number [10].

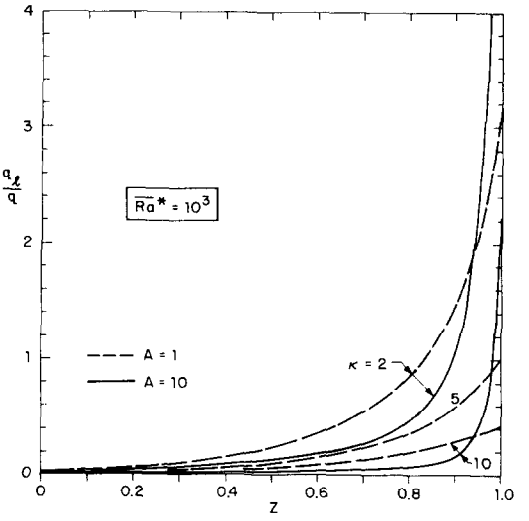

FIG. 5. Variation in local heat flux on the outer wall.

4.4. *Heat transfer results*

Based on the mean temperature difference $T_{m,i} - T_o$, an average Nusselt number on the inner wall is obtained as

$$Nu = 1/\theta_m = 1\Big/\int_0^1 \theta(0, Z)\, dZ. \tag{5}$$

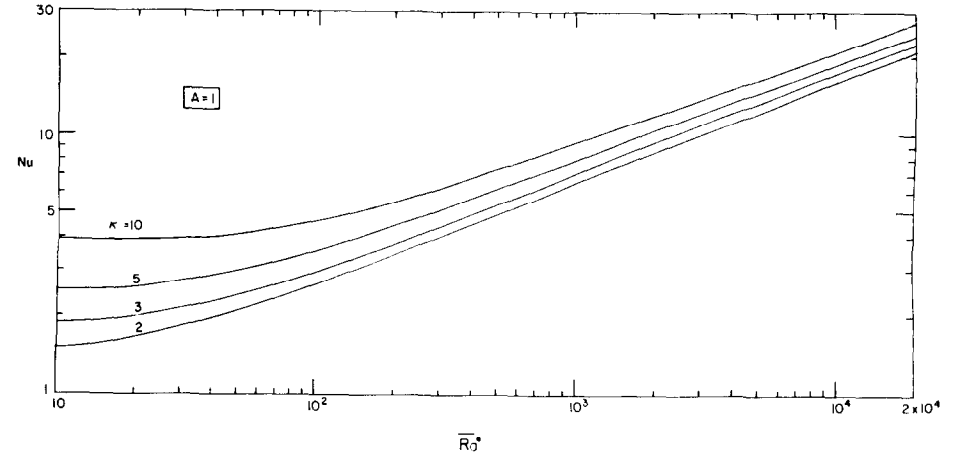

(a)

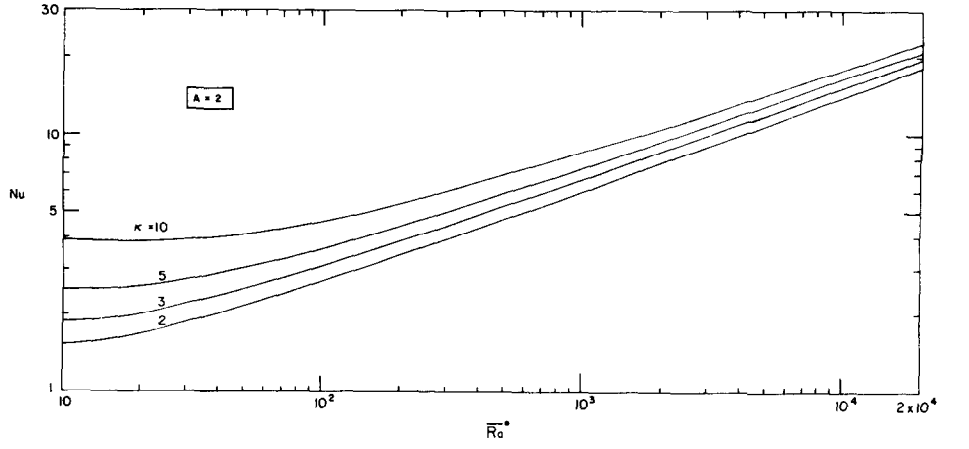

(b)

This Nusselt number can be directly used to compare the present heat transfer rates with those for the isothermally heated annulus by obtaining a Rayleigh number based on the mean temperature difference, $T_{m,i} - T_o$,

$$Ra^* = \overline{Ra}^*/Nu. \tag{6}$$

Secondly, this Nusselt number is also important for design purposes because it gives the mean temperature, θ_m, [equation (6)] which, in turn, provides the order of temperatures to be encountered for any particular values of $\overline{Ra}^*$, A and κ. The bounds of the temperature are then known.

Figures 6a–e present the average Nusselt number, Nu, for $A = 1$, 2, 5, 10 and 20. At very low Rayleigh numbers (conduction regime), the Nusselt number

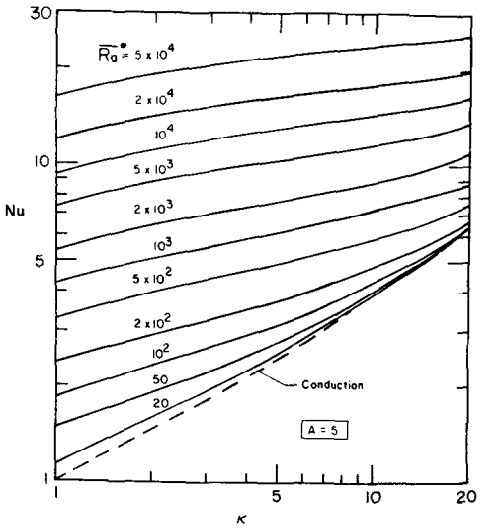

(c)

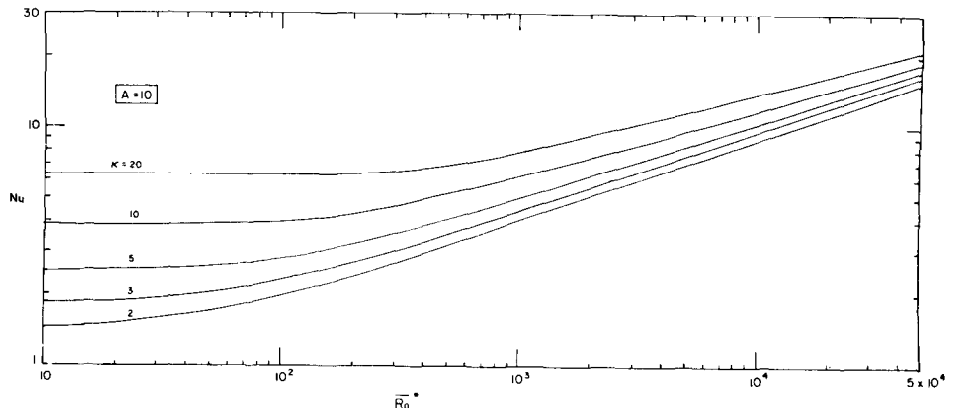

(d)

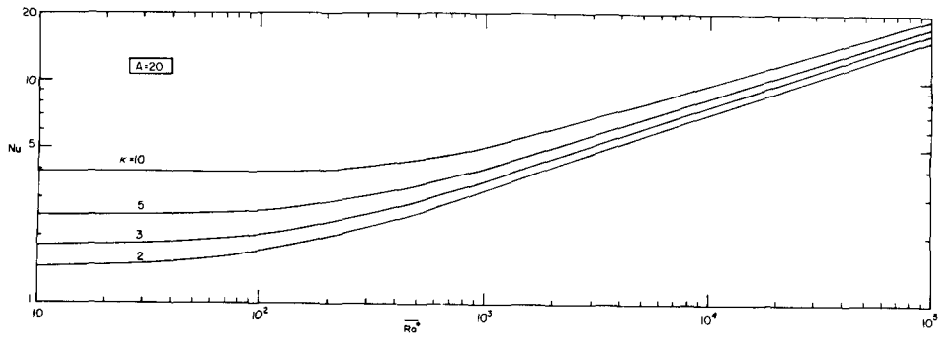

(e)

FIG. 6. Curvature effects on average Nusselt number, Nu, on the inner wall, (a) $A = 1$, (b) $A = 2$, (c) $A = 5$, (d) $A = 10$, and (e) $A = 20$.

approaches the conduction value, $(\kappa-1)/\ln(\kappa)$, for all aspect ratios. An increase in Rayleigh number is always associated with the increase in heat transfer rates, but the rate of increase strongly depends on the aspect and radius ratios, particularly for small Rayleigh numbers. The higher the values of A and κ, the lower is the rate of increase in Nu with $\overline{Ra}^*$ primarily because the flow regimes get extended (in terms of $\overline{Ra}^*$) when the aspect and radius ratios are increased [6]. In fact, Nu is almost constant up to $\overline{Ra}^* = 200$ when $A = 20$ and $\kappa = 10$ or $A = 10$ and $\kappa = 20$.

The above extension in the conduction and asymptotic flow regimes (refer to [13, 14] for the definitions) delays the start of the boundary-layer regime. The higher the aspect and/or radius ratios, the larger is the Rayleigh number required for the boundary-layer flow regime to start. The flow regime criteria for the isothermally heated annulus [6] can be conveniently used for the present problem without any appreciable error.

In the boundary-layer regime, the slope of the $\ln(Nu)$ vs $\ln(\overline{Ra}^*)$ curve is almost constant, though the effects of A and κ on this slope cannot be ruled out. It is thus possible to obtain a correlation as

$$Nu = C\,\overline{Ra}^{*m} A^{-n} \kappa^{p} \tag{7}$$

where exponents m, n and p, and constant C may depend on $\overline{Ra}^*$, A and κ. This correlation may further be modified to provide a relation between the Nusselt and Rayleigh numbers based on the temperature difference:

$$Nu = C_1\, Ra^{*r} A^{-s} \kappa^{t}, \tag{8}$$

where $C_1 = C^{1/(1-m)}$, $r = m/(1-m)$, $s = n/(1-m)$ and $t = p/(1-m)$.

Curvature effects. It is evident from Figs. 6a–e that the heat transfer rate increases with the curvature. This increase in the Nusselt number has been caused by the reduction in the effective sink temperature for the inner boundary layer when κ is increased beyond unity, and is consistent with the modifications in the temperature and flow fields (Section 4.1).

To characterize fully the curvature effects, the Nusselt numbers for $A = 5$ are plotted against κ in Fig. 6c. For pure conduction, the slope of this curve continually increases with κ. However, an increase in $\overline{Ra}^*$ reverses this behavior provided the aspect and radius ratios are not large such that the convective flow is in the conduction regime. For example, an increase in $\overline{Ra}^*$ from zero to 50 results in a substantial decrease in the slope at $\kappa = 1$, but when $\kappa > 15$, the slope is very close to that obtained for pure conduction (Fig. 6c). At high Rayleigh numbers, the slope of this curve continually decreases with an increase in κ provided the boundary-layer flow is maintained throughout.

Since the slope of $\ln(Nu)$ vs $\ln(\kappa)$ curve varies in a complex manner with $\overline{Ra}^*$, A and κ, this slope has been calculated for $1 \leqslant \kappa \leqslant 20$, and $A = 1$ and 10 and is presented in Table 3. It may be noted that this slope is equal to the exponent p in equation (7), and has been obtained by computing Nusselt numbers for two close values of κ corresponding to each radius ratio listed in Table 3. For pure conduction, p monotonically increases from 0.501 at $\kappa = 1$ to 0.719 at $\kappa = 20$, whereas an increase in $\overline{Ra}^*$ results in a decrease in p until the boundary-layer flow is established. For example, when $A = 10$ and $\kappa = 1$, p decreases to 0.296 at $\overline{Ra}^* = 10^3$, beyond which the change is minimal. For a square annulus, $A = 1$, the exponent p decreases to 0.3 at $\overline{Ra}^* = 10^4$, a value close to 0.296. When the radius ratio is increased beyond unity, the slope is found to be no longer constant at high $\overline{Ra}^*$. In fact, a close look at the decreasing p when $\overline{Ra}^*$ is increased, indicates that the exponent p asymptotically approaches a constant value for any fixed aspect and radius ratios. The asymptotic values of p are 0.296 and 0.269 for $\kappa = 1$ and 1.2, respectively. For $\kappa = 1.5$, it may be very close to 0.232. However, the present calculations do not provide the asymptotic value of p for $\kappa > 1.5$.

The effects of aspect ratio on the slope of $\ln(Nu)$ vs $\ln(\kappa)$ curve strongly depends on the convective flow regime or $\overline{Ra}^*$. If the Rayleigh number is very high such that the boundary-layer flow is maintained irrespective of the aspect ratio, the exponent p is observed to be a weak function of A. For example, when $\overline{Ra}^* = 10^4$ and $\kappa = 2$, p is equal to 0.208 and 0.203 for $A = 1$ and 10, respectively (Table 3). This is not true if the curvature effects are strong. At $\kappa = 4$, p is larger for $A = 10$ than that for $A = 1$. The difference further increases with an increase in κ, and is primarily because an increase in height-to-width ratio beyond a certain value reverses the boundary-layer flow regime to the asymptotic regime for fixed $\overline{Ra}^*$ and κ. The change in flow regime

Table 3. Slope of $\ln(Nu)$ vs $\ln(\kappa)$ curve [exponent p in equation (7)]

A	$\overline{Ra}^*/\kappa$	1	1.2	1.5	1.75	2	2.5	3	4	5	7	10	15	20
Conduction		0.501	0.515	0.534	0.546	0.557	0.575	0.590	0.612	0.629	0.653	0.677	0.702	0.719
1	10^2	0.307	—	0.295	—	0.296	0.299	0.303	0.311	0.328	0.377	0.429	0.470	0.487
	10^4	0.300	0.273	0.241	0.223	0.208	0.186	0.171	0.154	0.146	0.142	0.147	0.164	0.183
10	10^2	0.319	—	0.324	—	0.339	0.358	0.384	0.426	0.458	0.507	0.541	0.548	0.550
	10^3	0.296	—	0.243	—	0.234	0.224	0.232	0.245	0.263	0.289	0.350	0.413	0.457
	10^4	0.296	0.269	0.236	0.217	0.203	0.181	0.170	0.159	0.161	0.169	0.198	0.238	0.276
	10^5	0.296	0.269	0.232	0.209	0.191	0.164	0.146	0.124	0.114	0.109	0.116	0.138	0.160

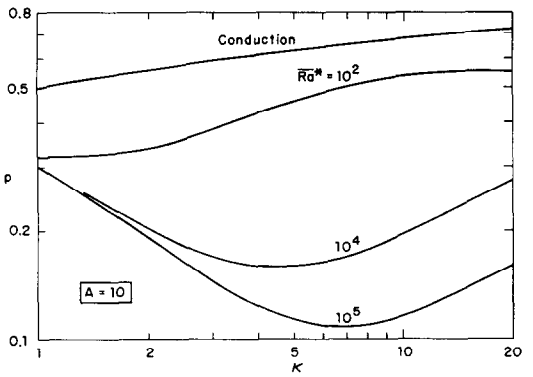

FIG. 7. Variation in exponent p [equation (7)] with the radius ratio.

from the boundary layer to asymptotic, with an increase in A is well established in literature for the vertical cavities, $\kappa = 1$ [13].

An interesting aspect of the curvature effects is the strong dependence of p on the radius ratio. Though p always increases with κ at $\overline{Ra}^* = 0$, the behavior is just the reverse when the Rayleigh number is high. In the boundary-layer regime, the slope p is observed to decrease with an increase in κ; p being largest at $\kappa = 1$ (Fig. 7 and Table 3). When $\overline{Ra}^* = 10^5$ and $A = 10$, p asymptotically decreases from 0.296 at $\kappa = 1$ to 0.109 at $\kappa = 7$ whereas for $\overline{Ra}^* = 10^4$ and $A = 1$, the change in p is from 0.3 to 0.142. This clearly implies that the rate of increase in the Nusselt number diminishes with an enhancement in the curvature effects. However, the exponent p does not decrease forever. In fact, p starts increasing when the radius ratio is increased beyond a certain value (Table 3 and Fig. 7). This reversal in the diminishing effect of κ is caused by the change in the flow regime from the boundary layer to asymptotic. The critical radius ratio for this change in the flow regimes is characterized by $\partial p/\partial \kappa = 0$, and is a strong function of $\overline{Ra}^*$ and A. The smaller the Rayleigh number and/or the higher the aspect ratio, the smaller is the value of this critical radius ratio.

Fortuitously, the curves for ln (p) vs ln (κ) exhibit straight line behavior (Fig. 7) when $\overline{Ra}^*$ is large and κ is small, i.e. when the flow is in the boundary-layer regime. A correlation for p may thus be obtained as

$$p = 0.305\kappa^{-0.676}, \quad \kappa < 4 \tag{9}$$

for $\overline{Ra}^* = 10^5$ and $A = 10$. The above correlation predicts the tabulated values of p within 0.7% except for $\kappa = 1$ where the difference is 3%. At $\kappa = 4$, the predicted value is 4% lower than the numerical value.

The above equation (9) presents a simple and explicit relation between p and κ. Though this type of expression is always sought, it is difficult to obtain a generalized correlation for wide range of parameters since the constant and the exponent in equation (9) are complex functions of $\overline{Ra}^*$, A and κ. This strong dependence of p on κ is contrary to the observation of Thomas and De Vahl Davis [14] and others that p is a constant for the natural convection in a fluid-filled, vertical annulus. Furthermore, the Rayleigh number at which the flow regime changes, also depends on the radius ratio. For fixed values of $\overline{Ra}^*$ and A, the boundary-layer flow regime at $\kappa = 1$ changes to the asymptotic regime and then to the conduction regime as the radius ratio is increased. This also does not agree with the observation [14] that the flow regime criteria are independent of the radius ratio.

Effects of aspect ratio. As is well-established, the Nusselt number for a vertical cavity ($\kappa = 1$) decreases with an increase in the aspect ratio beyond a certain value between 0.5 and 2, which is a function of the Rayleigh number [13]. The higher the Rayleigh number, the lower is the aspect ratio for $(Nu)_{max}$. A change in the heated wall boundary condition from the constant temperature to the uniform heat flux does not produce any appreciable effects on this behavior [10]. Evidently, the slope of ln (Nu) vs ln (A) curve or the exponent n in equation (7) for fixed $\overline{Ra}^*$ and κ, is zero at $A_{critical}$.

To visualize the effects of radius ratio on the functional relationship of Nusselt number with A, the exponent n has been listed in Table 4 for $\kappa = 1$ and 10. It is observed that the critical aspect ratio for $(Nu)_{max}$ is less than unity when $\overline{Ra}^* = 10^4$ and $\kappa = 1$. An increase in the radius ratio for fixed $\overline{Ra}^*$ further reduces the value of $A_{critical}$ (Table 4, also [7]). Furthermore, the absolute value of n always increases with the aspect ratio when the flow is in the boundary-layer regime (Table 4). The rate of increase in n, i.e. $\partial n/\partial A$, is highest at $A_{critical}$ and is observed to decrease when the height-to-width ratio increases. This reduction in $\partial n/\partial A$ is essentially a result of the diminishing end effects at higher aspect ratios. In fact, n increases from 0.092 at $A = 1$ to 0.342 at $A = 50$ when $\kappa = 1$. It may be noted that Prasad and Kulacki [10] have reported an average value of $n = 0.328$ based on the computations for $A = 5$, 10, 20 and 50.

Table 4. Slope of ln (Nu) vs ln (A) curve [exponent n in equation (7)]

κ	$\overline{Ra}^*/A$	1	1.5	2	3	4	5	7	10	20	50
1	10^4	0.092	0.188	0.237	0.277	0.295	0.307	0.317	0.323	0.333	0.342
	10^3	0.012	0.106	0.165	0.201	0.226	0.230	0.236	0.226	0.203	0.151
10	10^4	0.131	0.205	0.240	0.264	0.275	0.282	0.285	0.285	0.283	0.272
	10^5	0.205	0.249	0.272	0.289	0.297	0.301	0.305	0.301	0.297	0.295

An increase in κ results in higher values of n for fixed $\overline{Ra}^*$ and A. However, the asymptotic relationship between n and A does not change as long as the boundary-layer flow is maintained. Once, both the aspect and radius ratios are large such that the flow is no more in the boundary-layer regime for given $\overline{Ra}^*$, the slope n starts decreasing. The gradient $\partial n/\partial A = 0$ may thus characterize the change in flow regime from the boundary layer to asymptotic.

4.5. *Comparison with cylinder solutions*

As already reported [6, 7], the heat transfer rate for an annulus asymptotically approaches that for a vertical cylinder embedded in an infinite medium at T_0 when the radius ratio is increased beyond unity. This behavior is consistent with the observed effects of curvature on the temperature field. As noted earlier, the effective sink temperature for the inner boundary layer decreases very fast with an increase in κ, approaching very close to T_0 at large values of κ. Evidently, the effect of the outer wall on the heat transfer at the inner surface is minimal at large radius ratios. This diminishing effect of the presence of outer wall is also exhibited in Fig. 6c where $p \to$ a constant value when $\kappa \to \infty$. However, for the annulus results to be close to the cylinder solutions, the end effects should be small. In can thus be expected that the difference between the two results will decrease as $A \to \infty$. It is important to note that the above behavior is true only when the convective flow is in the boundary-layer regime.

To substantiate the above qualitative discussions and to study the effects of $\overline{Ra}^*$, A and κ on this aspect of the annulus results, the heat transfer results are compared with the cylinder solutions obtained from Minkowycz and Cheng [15] in Figs. 8a and b. Here, $(Nu)_{cyl}$ is observed to be 29% higher than Nu when $\kappa = 2$, $A = 10$ and $Ra^* = 10^3$. The variation reduces to only 10% at $\kappa = 5$ and to 2.2% at $\kappa = 20$. However, the difference at $\kappa = 20$, increases to 16% when the Rayleigh number is reduced to 110. These results clearly exhibit that $Nu \to (Nu)_{cyl}$ when Ra^* and $\kappa \to \infty$. As noted earlier, the slope of ln (Nu) vs ln (κ) curve, p, decreases logarithmically [equation (9)], i.e. p asymptotically approaches zero as $\kappa \to \infty$. It is interesting to note that a similar behavior is exhibited by the solutions for the embedded cylinder [15].

The effect of aspect ratio on the difference between Nu and $(Nu)_{cyl}$ can be observed in Fig. 8b. Here, $(Nu)_{cyl}$ is 25% higher than Nu when $Ra^* = 500$, $\kappa = 10$ and $A = 1$. The agreement is within 6% at $A = 5$, and within 13% at $A = 20$. It may thus be concluded that $Nu \to (Nu)_{cyl}$ as the aspect ratio is increased. A larger difference at $A = 20$ is essentially due to the fact that $Ra^* = 500$ is not sufficient to maintain the boundary-layer flow at $\kappa = 10$ and $A = 20$. In fact, an increase in Ra^* to 5×10^3 reduces the difference to only 5% at $A = 20$. Hence, the higher the aspect ratio, the smaller is the difference between Nu and $(Nu)_{cyl}$. The only constraint to this behavior is that the boundary-layer flow must exist on the inner wall. From these results (Figs. 8a and b), it is easy to conclude that the Nusselt number for the annulus is very close to that for the embedded cylinder when $Ra^* > 500$, $A > 5$ and $\kappa > 10$ provided the flow is in the boundary-layer regime.

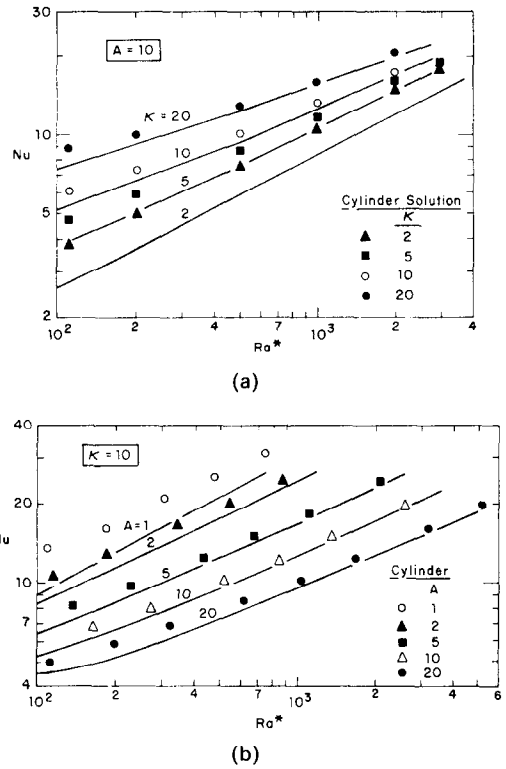

FIG. 8. Annulus results compared with the cylinder solutions [15] for (a) $A = 10$, and (b) $\kappa = 10$.

4.6. *Constant temperature vs constant heat flux*

To characterize the effects of heated wall boundary condition on the overall heat transfer rate, the present Nusselt numbers are compared with those for the isothermally heated annuli in Figs. 9a and b. As expected, the two Nusselt numbers are equal when the flow is in the conduction regime. An increase in Rayleigh number enhances the heat transfer rates for both types of heating, but the rate of increase is larger in the case of constant heat flux. This agrees with the general observation that the Nusselt number for a cavity is higher for the uniform heat flux boundary condition [10]. It must be noted that the above conclusion is based on the consideration that $(T_{m,i} - T_0)$ is equal to $(T_{iso} - T_0)$. The higher rate of heat transfer in the present case, is consistent with the modification in temperature field owing to a change in the boundary condition from the constant temperature to a constant heat flux.

For fixed values of A and κ, the ln (Nu) vs ln (Ra^*) curves for the two types of heating are observed to be almost parallel beyond a certain Rayleigh number (Figs. 9a and b). It is thus evident that the exponent r in equation (8) is a weak function of the heated wall

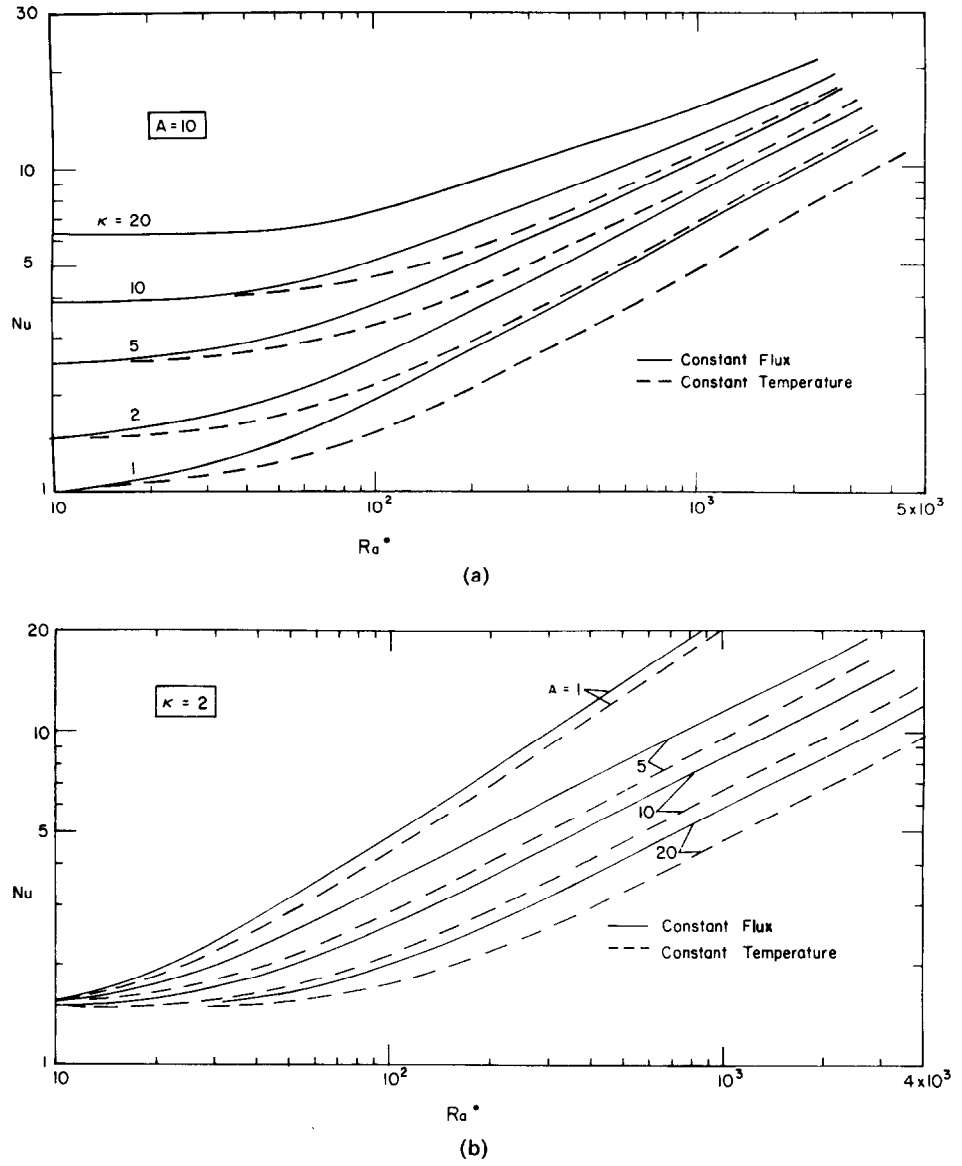

FIG. 9. Effects of the heated wall boundary conditions on Nusselt number (a) $A = 10$, and (b) $\kappa = 2$.

boundary condition once the flow is in the boundary-layer regime. The Nusselt number plots for various values of A and κ (Figs. 9a and b) further indicate that the aspect and radius ratios do not have any appreciable effect on the exponent r. In fact, for a tall cavity ($A > 2, \kappa = 1$) heated by applying a uniform heat flux, Prasad and Kulacki [10] have obtained $r = 0.527$ which is very close to the value of r (0.52 or 0.5) for the isothermal heating [6 and others].

It can further be observed from Fig. 9a that the difference between Nu and Nu_{iso} decreases with an increase in the radius ratio. For $A = 10, Ra^* = 10^3$ and $\kappa = 1$, Nu is 30% higher than Nu_{iso} whereas the difference is only 12% when κ is increased to 10. This has directly followed from the temperature distribution on the inner wall. In Fig. 4b, the temperature gradient, $\partial\theta_w/\partial Z \to 0$ as $\kappa \to \infty$ except for small distances from the top and bottom edges. Thus, the asymmetries in the flow, due to the constant flux boundary condition, become indistinct when $\kappa \to \infty$.

The effect of aspect ratio on $(Nu - Nu_{iso})$ is just the reverse. The higher the aspect ratio, the larger is Nu compared to Nu_{iso}. For $\kappa = 2$ and $Ra^* = 800$, Nu is 9% higher than Nu_{iso} at $A = 1$. When A is increased to 5, the difference is 22% which further increases to 28% at $A = 20$. These variations in $(Nu - Nu_{iso})$ clearly indicate that the exponents s and t in equation (2) depend on the heated wall boundary condition.

4.7. *Heat transfer correlations*

Generalized heat transfer correlations of the form of equations (7) and (8) are always important for design

Table 5. Exponents m and n, and constant $\bar{C}$ for equation (10)

κ	A	$\bar{C}$	m	n	$\overline{Ra}^* \geqslant$	Maximum % error
	1	0.312	0.413	0	100	1.66
1†	2	0.411	0.368	0	100	0.75
	$5 \leqslant A \leqslant 50$	0.662	0.345	0.328	500	2.00
	1	0.430	0.393	0	100	1.00
2	2	0.520	0.359	0	100	0.58
	$5 \leqslant A \leqslant 20$	0.812	0.339	0.319	500	1.60
	1	0.512	0.382	0	100	1.97
3	2	0.589	0.354	0	200	0.29
	$5 \leqslant A \leqslant 20$	0.917	0.333	0.311	500	2.01
	1	0.617	0.371	0	200	1.21
5	2	0.719	0.340	0	200	0.69
	$5 \leqslant A \leqslant 20$	1.096	0.320	0.301	500	1.69
	1	0.873	0.344	0	200	2.31
10	2	0.989	0.316	0	500‡	0.73
	$5 \leqslant A \leqslant 20$	1.512	0.293	0.279	1000	2.42
20	$5 \leqslant A \leqslant 10$	2.052	0.269	0.244	1000	3.10

† Results for vertical cavity ($\kappa = 1$) are taken from ref. [10].
‡ For $A > 10$, $\overline{Ra}^* \geqslant 10^3$.

purposes, and any studies such as the present one attempt to obtain them. But the task is not easy in the present case owing to complex functional relationship between the exponents and the governing parameters. However, an equation of the form:

$$Nu = \bar{C}\,\overline{Ra}^{*m} A^{-n}, \quad \text{for a fixed } \kappa \qquad (10)$$

has been used to correlate the present results for $\kappa = 1$, 2, 3, 5 and 10. The values of m, n and $\bar{C}$ are presented in Table 5 with the range of Rayleigh number and aspect ratio to which they are applicable.

5. CONCLUSION

Numerical results for the natural convection in a vertical, porous annulus with the constant heat flux on the inner wall, indicate the following:

1. Introduction of curvature disturbs the centro-symmetric properties of the isothermally heated, vertical cavity and results in lower effective sink temperature for the heated wall boundary layer. It enhances the stratification in the upper region of the enclosure and results in higher velocities near the top edge of cold wall. A change in the boundary condition from the constant temperature to the constant heat flux further strengthens this behavior.
2. The heated wall temperature, θ_w, increases with Rayleigh number but the change in actual temperature T_w depends on how $\overline{Ra}^*$ is changed. The temperature θ_w at any location decreases with an increase in radius ratio, but increases with the aspect ratio.
3. The peak temperature, $(\theta_w)_{max}$ increases with the Rayleigh number whereas the radius ratio affects it in an opposite manner. However, there exists an aspect ratio as a function of $\overline{Ra}^*$ and κ for which this peak temperature is maximum. The upper bound for this temperature is $2\theta_m$, for $1 \leqslant A \leqslant 20$.
4. The overall Nusselt number increases with an increase in the radius ratio, but the rate of increase diminishes as $\kappa \to \infty$. The exponent of κ in equation (7), p, is a complex function of $\overline{Ra}^*$, A and κ. In the boundary-layer regime, p decreases logarithmically with the increase in κ.
5. The above diminishing effect of κ brings annulus results close to the cylinder solutions provided the flow is in the boundary-layer regime. Generally, the two results can interchangeably be used with a reasonable accuracy for $Ra^* > 500$, $A > 5$ and $\kappa > 10$.
6. The heat transfer rate for the constant flux case is higher than that for the isothermal heating. In boundary-layer regime, the difference $(Nu - Nu_{iso})/Nu_{iso}$ is almost constant. But an increase in the aspect ratio enhances this difference whereas the radius ratio has an opposite effect.

REFERENCES

1. C. E. Hickox and D. K. Gartling, A numerical study of natural convection in a vertical annular porous layer, ASME Paper No. 82-HT-68 (1982).
2. M. A. Havstad and P. J. Burns, Convective heat transfer in vertical cylindrical annuli filled with a porous medium, *Int. J. Heat Mass Transfer* **25,** 1755–1766 (1982).
3. J. R. Philip, Axisymmetric free convection at small Rayleigh number in porous cavities, *Int. J. Heat Mass Transfer* **25,** 1689–1699 (1982).
4. D. C. Reda, Natural convection experiments in a liquid saturated porous medium bounded by vertical coaxial cylinders, *J. Heat Transfer* **105,** 795–802 (1983).
5. M. Keyhani, V. Prasad and F. A. Kulacki, An approximate analysis for thermal convection with application to vertical annulus, *Chem. Eng. Commun.*, in press.
6. V. Prasad and F. A. Kulacki, Natural convection in a vertical porous annulus, *Int. J. Heat Mass Transfer* **27,** 207–219 (1984).
7. V. Prasad and F. A. Kulacki, Natural convection in

porous media bounded by short concentric vertical cylinders, *J. Heat Transfer* **107**, 147–154 (1985).
8. V. Prasad, F. A. Kulacki and M. Keyhani, Natural convection in porous media, *J. Fluid Mech.* **150**, 89–119 (1985).
9. V. Prasad, F. A. Kulacki and A. V. Kulkarni, Free convection in a vertical porous annulus with constant heat flux on the inner wall—experimental results, *Int. J. Heat Mass Transfer* **29**, 713–723 (1986).
10. V. Prasad and F. A. Kulacki, Natural convection in a rectangular porous cavity with constant heat flux on one vertical wall, *J. Heat Transfer* **106**, 152–157 (1984).
11. A. D. Gosman, W. M. Pun, A. K. Runchal, D. B. Spalding and M. Wolfshtein, *Heat and Mass Transfer in Recirculating Flows*. Academic Press, New York (1969).
12. P. J. Roache, *Computational Fluid Dynamics*. Hermosa, Albuquerque, NM (1982).
13. V. Prasad and F. A. Kulacki, Convective heat transfer in a rectangular porous cavity—effect of aspect ratio on flow structure and heat transfer, *J. Heat Transfer* **106**, 158–165 (1984).
14. R. W. Thomas and G. de Vahl Davis, Natural convection in annular and rectangular cavity—a numerical study, *Proc. 4th Int. Heat Transfer Conference*, Paris, Vol. 4, NC 2.4. Elsevier, Amsterdam (1970).
15. W. J. Minkowycz and P. Cheng, Free convection about a vertical cylinder embedded in a porous medium, *Int. J. Heat Mass Transfer* **19**, 805–813 (1976).

ETUDE NUMERIQUE DE LA CONVECTION NATURELLE DANS UN ESPACE ANNULAIRE POREUX ET VERTICAL AVEC FLUX SURFACIQUE CONSTANT SUR LA PAROI INTERNE

Résumé—Des solutions numériques de convection naturelle dans un espace annulaire vertical, poreux sont données pour le cas de la paroi interne chauffée à densité de flux uniforme. Ces conditions conduisent à un transfert thermique plus grand que pour le chauffage isotherme. Plus grand est le rapport de forme, plus marquée est cette différence tandis que l'effet du rapport des rayons est contraire. Bien que le transfert augmente avec la courbure, l'exposant p dans $Nu = C\,\overline{Ra}^{*m} A^{-n} \kappa^{p}$ est une fonction forte du rapport des rayons κ. Dans le régime de couche limite, p décroît logarithmiquement à partir d'une valeur maximale pour $\kappa = 1$. Ceci amène les résultats de l'espace annulaire proches de ceux du cylindre pour les grands rapports des rayons. Le pic de température dans l'enceinte ne dépasse jamais deux fois la température moyenne.

NUMERISCHE UNTERSUCHUNG DER NATÜRLICHEN KONVEKTION IN EINEM PORÖSEN RINGRAUM MIT KONSTANTEM WÄRMESTROM AN DER INNENWAND

Zusammenfassung—Für die natürliche Konvektion in einem senkrechten, porösen Ringraum werden für den Fall konstanten Wärmestroms an der Innenwand numerische Lösungen angegeben. Im Vergleich zur isothermen Innenwand führt diese Anordnung zu einem verbesserten Wärmeübergang. Je größer das Verhältnis von Höhe zu Spaltweite ist, desto größer wird die Differenz zwischen den beiden Fällen; dagegen bewirkt eine Vergrößerung des Verhältnisses von Außen- zu Innenradius das Gegenteil. Obwohl der Wärmeübergang mit zunehmender Krümmung besser wird, ist der Exponent p in der Gleichung $Nu = C\,\overline{Ra}^{*m} A^{-n} \kappa^{p}$ stark vom Radienverhältnis κ abhängig. Im Grenzschichtbereich nimmt p logarithmisch ab, sein Maximum liegt bei $\kappa = 1$. Dies führt dazu, daß die Ergebrisse für den Ringraum für große Radienverhältnisse denen beim Zylinder gleichen. Die maximale Temperatur im Ringraum übersteigt die mittlere nie um mehr als einen Faktor 2.

ЧИСЛЕННОЕ ИССЛЕДОВАНИЕ ЕСТЕСТВЕННОЙ КОНВЕКЦИИ В ВЕРТИКАЛЬНОМ ПОРИСТОМ КОЛЬЦЕВОМ СЛОЕ С ПОСТОЯННЫМ ТЕПЛОВЫМ ПОТОКОМ НА ВНУТРЕННЕЙ СТЕНКЕ

Аннотация—Численные решения задачи естественной конвекции в вертикальном пористом кольцевом слое представлены для случая, когда внутренняя стенка нагревается постоянным тепловым потоком. Это приводит к большей скорости теплообмена по сравнению с изотермическим нагревом, причем различие тем больше, чем больше отношение высоты к радиусу, в то время как отношение радиусов оказывает обратное влияние. Хотя скорость теплопереноса увеличивается с кривизной, показатель степени p в выражении $Nu = CRa^{*m} A^{-n} \kappa^{p}$ существенно зависит от отношения радиусов κ. В режиме пограничного слоя p уменьшается логарифмически от максимального значения, соответствующего $\kappa = 1$. Это сближает результаты для кольцевого слоя при больших отношениях радиусов с данными для цилиндра. Максимум температуры в замкнутом объеме никогда не превышает удвоенную среднюю температуру.